H trapping and mobility in nanostructured tungsten grain boundaries: a combined experimental and theoretical approach

2015 Nucl. Fusion 55 113009

(http://iopscience.iop.org/0029-5515/55/11/113009)

IOP Publishing | International Atomic Energy Agency Nuclear Fusion

Nucl. Fusion **55** (2015) 113009 (9pp) doi:10.1088/0029-5515/55/11/113009

H trapping and mobility in nanostructured tungsten grain boundaries: a combined experimental and theoretical approach

C. González[1,2], M. Panizo-Laiz[1], N. Gordillo[1], C.L. Guerrero[1], E. Tejado[3,4], F. Munnik[5], P. Piaggi[6], E. Bringa[7], R. Iglesias[2], J.M. Perlado[1] and R. González-Arrabal[1]

[1] Instituto de Fusión Nuclear, ETSI de Industriales, Universidad Politécnica de Madrid, C/José Gutierrez Abascal, 2, E-28006 Madrid, Spain
[2] Departamento de Física, Universidad de Oviedo, E-33007 Oviedo, Spain
[3] Departamento de Ciencia de Materiales, ETSI Caminos, Canales y Puertos, Universidad Politécnica de Madrid, E-28040 Madrid, Spain
[4] Centro Nacional de Investigaciones Metalúrgicas (C.S.I.C.), Avda. de Gregorio del Amo 8, E-28040 Madrid, Spain
[5] Helmholtz-Zentrum Dresden-Rossendorf, PO Box 10119, D-01314 Dresden, Germany
[6] Instituto Sábato, UNSAM/CNEA, Avda. Gral. Paz 1499, 1650 San Martín, Argentina
[7] Facultad de Ciencias Exactas y Naturales, Universidad Nacional de Cuyo, Mendoza 5500, Argentina

E-mail: cesar.gonzalez.pascual@gmail.com

Received 25 May 2015, revised 21 July 2015
Accepted for publication 11 August 2015
Published 8 September 2015

Abstract

The trapping and mobility of hydrogen in nanostructured tungsten grain boundaries (GBs) have been studied by combining experimental and density functional theory (DFT) data. Experimental results show that nanostructured W coatings with a columnar grain structure and a large number of (1 1 0)/(2 1 1) interfaces retain more H than coarsed grained W samples. To investigate the possible influence of GBs on H retention, a complete energetic analysis of a non-coherent W(1 1 0)/W(1 1 2) interface has been performed employing DFT. Our results show that this kind of non-coherent interface largely attracts point defects (both a H atom and a metallic monovacancy separately) and that the presence of these interfaces contributes to a decrease in the migration energy of the H atoms with respect to the bulk value. When both the W monovacancy and H atom are introduced together into the system, the HV complex becomes the most stable configuration and one of the mechanisms explaining the H retention in the radiation damaged GB observed experimentally.

Keywords: nanostructured W, grain boundaries, H trapping and mobility, defects

(Some figures may appear in colour only in the online journal)

1. Introduction

Energy production and the combat against climate change are at the centre of our daily concerns and stand for a socio-economic priority. Nowadays, great efforts are being made to develop different ways of providing clean energy sources to supply our increasing energy demand abating provisions of fossil fuels. Among them, nuclear fusion is one of the most promising options presenting large advantages such as high energy efficiency, reliable power, plentiful fuel and increased safety.

Currently, two main approaches for nuclear fusion energy production are being studied: magnetic confinement (MC) and inertial, also called laser, confinement (IC). The large-scale project for MC studies is the international thermonuclear experimental reactor (ITER) [1] supported by a multinational consortium (EU, Japan, USA, Korea, Russian, China and India). Concerning IC, the largest projects are the laser inertial

fusion engine (LIFE) [2] reactor in USA and the High Power laser Energy Research (HiPER) [3] in the EU. The aim of these projects is to demonstrate the scientific and technological feasibility of controlled fusion. Nevertheless, a very important question, which has to be addressed in the context of these reactors, is the choice of the plasma facing material (PFM). Because of its excellent properties, tungsten is one of the most attractive materials proposed in nuclear fusion reactors [4–8]. However, it is known that the irradiation of tungsten with H leads to surface blistering and subsequent cracking and exfoliation [9, 10]. Blister characteristics and cracking behavior of tungsten under hydrogen irradiation has been observed to strongly depend on irradiation conditions and on microstructures [11, 12, 21]. In general, the H blistering in polycrystalline W has been related to its retention and accumulation at intrinsic defects such as vacancies, grain boundaries (GBs) or dislocations.

One option to delay the appearance of blistering and exfoliation effects is the use of nanostructured materials [22–24]. The behavior of these materials under irradiation is very much dominated by the large density of GBs, which at room temperature (RT) act as (i) annihilation centres for Frenkel pairs (self-healing behavior) [25, 26] and (ii) pinning centres for hydrogen [27, 28]. These two facts may drive the delay, i.e. a shift to higher irradiation fluences, of the formation of blisters which is very relevant from the application point of view. Because of this reason, the study of the role of GBs in hydrogen behavior is very relevant.

One of the main areas of research related to development and characterization of nanomaterials is described in the W and W-alloys program of the European fusion development agreement (EFDA) topical group on Fusion Materials [13]. Here Rieth *et al* describe the recent progress done to produce, to characterize and to simulate the behavior of diverse nanoestrcutured pure W [14], and W-alloys, such as W-Ti, W-Ta, and reinforced with Y_2O_3 [15], La_2O_3 [16] or TiC [17] nanoparticles for different purposes, for example, to develop a structural material with improved mechanical properties [18, 19] or to improve security in the case of an accidental loss of coolant [20]. However, to the best of our knowledge, only a few works have been devoted so far, to study the behavior of light species and in particular of H, in nanostructured W.

Experimental data evidences that the retention of hydrogen in nanostructured tungsten (NW) is larger than in coarse grained tungsten (CGW) [29] and that hydrogen is pinned at GBs in a recrystallized tungsten sample [30]. Computer simulations, based on DFT and Molecular Dynamics (MD) carried out hitherto, indicate that GBs can behave as trapping centers for hydrogen and therefore hydrogen strongly segregates to them [31, 32]. It has also been shown that GBs may act as fast transport channels due to the presence of low-activation-energy migration paths, possibly leading to enhanced diffusion rates for hydrogen in the trace impurity limit. However, it is worthwhile to mention that previous DFT simulations have been performed for ideal GBs, i.e. only coherent interfaces have been considered. For example, Zhou *et al* studied in detail the $36.9°[1\,0\,0]\{0\,1\,3\}\Sigma = 5$ symmetrical tilted GB [31], while Xiao and Geng focused their analysis in the $\Sigma = 3\langle 1\,1\,1\rangle$ tilt grain boundary [35]. A recent work has been devoted to the study of general high-angle GBs in nanocrystalline W using MD simulations [32]. Their findings indicate that hydrogen diffusivity for NW samples is lower than that reported for CGW and furthermore, it strongly depends on hydrogen concentration. It was also found that trapping energies in general high-angle GBs are higher than those previously calculated for high-symmetry GBs in bicrystals [33]. The differences between these data show the need of study the influence of every particular defect in the hydrogen behavior. Thus, as previously stated by Lu *et al* [34] there is a large necessity of combining modeling and experiments to account for the role of each kind of defect in the hydrogen behavior, which is required to validate simulations and to use them for further realistic predictions of material behavior under conditions which experimentally cannot be reached so far like those taking place in a nuclear fusion reactor.

The aim of this paper is to study the hydrogen behavior in a particular grain boundary. For this purpose, we carried out DFT calculations for a realistic non-coherent interface formed by two W(1 1 0) and W(1 1 2) surfaces as suggested experimentally. The stability and mobility of a H atom as well as a metallic vacancy at the interface are analyzed in detail. Our results show that both defects are highly attracted by the interface and that they can find easier ways to migrate along the GB than inside the perfect bulk.

2. Methodology

2.1. Experimental details

W coatings with a thickness of $\sim$1.2 μm and root mean square (rms) roughness lower than 3 nm were deposited by DC sputtering from a pure W commercial target (99.95%) at a normal incidence angle on single-side polished Si (1 0 0) substrate. More details about sample fabrication are reported in [36].

In order to study the influence of the microstructure of the sample on the behavior of hydrogen, two samples, one with a columnar structure, the so-called nanostructured tungsten (NW), with an average diameter of $\sim$100 nm and a commercial coarse grained W (CGW) with a grain size in the μm range were implanted with H at room temperature (RT). Implantations were performed at the ion implanter located at the Helmholtz Zentrum Rossendorf Dresden. The implantation energy and the fluence were selected to be 170 keV and 5×10^{20} m^2 in order to mimic IC energies in HiPER [37].

Prior to implantation, the CGW samples were mechanically polished by using napless synthetic cloth. For the first rough polishing step, a 0.5 μm colloidal alumina was used. The second polishing was done by using a 0.03 μm colloidal alumina. No other treatment was applied to the CGW before implantation. The sample morphology was characterized prior to and after implantation by high resolution field emission gun-scanning electron microscope (FEG-SEM) operated at different acceleration voltages from 1 to 3 kV.

The microstructural characterization of the samples prior to and after implantation was investigated by x-ray diffraction

(XRD) using a Philips X-PERT four cycle diffractometer with a Cu $K\alpha$ radiation source. The XRD measurements were performed in the Bragg–Brentano geometry.

The H depth profiles were characterised by resonance nuclear reaction analysis (RNRA) experiments, carried out by using the $H(^{15}N,^{4}He\gamma)^{12}C$ [38] nuclear reaction with a N^{2+} beam impinging onto the sample surface at normal incidence. The beam energy was varied in the range from 6.425 to 11.033 MeV. The γ-rays were detected by a 10×10 cm^2 bismuth germinate detector mounted immediately outside the vacuum chamber at about 1.5 cm behind the sample. Some special precautions were taken in order to carry out reliable depth profiling measurements and to avoid ion beam-induced hydrogen diffusion [39]. The beam spot and the current were selected to be 2×2 mm^2 and $\sim$10 nA, respectively. In addition, the beam spot position was changed every two measurements. As described in [40], in order to assure that the selected experimental configuration does not lead to ion beam-induced diffusion, several spectra were sequentially measured on the same point up to a dose 10 times higher than that used in these experiments. No ion beam-induced hydrogen diffusion was detected in any case. More details about RNRA characterization are given in [29].

2.2. Theoretical simulations

DFT simulations were performed with the *Vienna Ab initio Simulation Package* VASP code [41]. The Perdew–Burke–Ernzerhof (PBE) parameterization [42] of the generalized gradient approximation (GGA) for the exchange and correlation functional was used as well as the Plane Augmented Wave pseudopotentials provided by the code [43]. Six valence electrons have been considered for W (4 *3d* and 2 *4s*) and one single *1s* valence electron for H. Within these approximations, the lattice parameter was estimated to be 3.172 Å for the cutoff energy of 400 eV used for the plane waves, in good agreement with the experimental value of 3.165 Å [44].

The experimental data suggest (see the following section) that W/W interfaces are created by placing two W(1 1 0) and W(1 1 2) surfaces in front of each other. Unfortunately, nothing is known about the most favorable relative orientations. Figure 1 shows two ideal interfaces built with the lattice parameter obtained with VASP. The light (dark) blue spheres represent the W atoms in the (1 1 2) [(1 1 0)] surface. The atomic configuration of the (1 1 0) surface in figure 1(*b*) is rotated 55 degrees with respect to that in figure 1(*a*). Both reconstructions are non-coherent and, consequently, the surfaces do not fit perfectly. For this reason, one of them (the (1 1 2)) had to be slightly expanded ($\sim$1%) (see the direction indicated by the red arrow in both interfaces shown in figure 1) when periodic boundaries are included in the relaxation of the system. The red dotted lines define the two dimensional supercells accessible to DFT simulations. The following calculations presented in this work are refereed to the interface shown in figure 1(*b*).

As recently suggested [45], it is highly recommended to include at least 6 layers of each surface to perform a DFT simulation of this kind of interfaces as it is shown in figure 2.

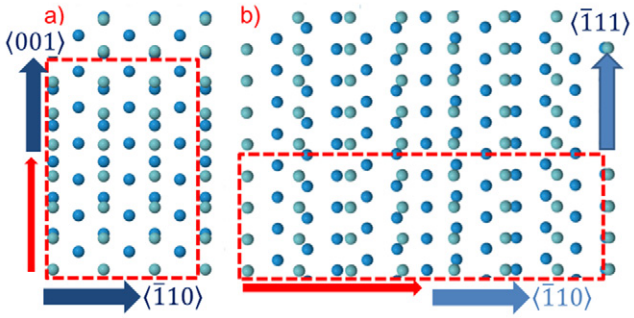

Figure 1. (*a*) and (*b*) Two relative orientations of the W(1 1 2)/W(1 1 0) interface. The structure shown in (*b*) is analyzed in detail in this work.

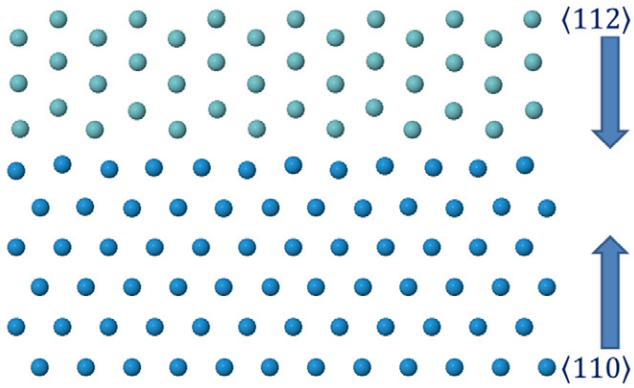

Figure 2. Lateral view of the slab used in the simulation. Light and dark blue spheres correspond to the (1 1 2) and (1 1 0) surfaces, respectively.

Following this recommendation, both surfaces were firstly relaxed separately. After that, they were joined by setting an initial distance between both surfaces of 2.24 Å, that is the same as the interlayer distance in the ⟨1 1 0⟩ direction, including a free vacuum of 12 Å. Subsequently, the complete slab was fully relaxed until the atomic forces were lower than 0.025 eV Å^{-1}. The last layer of each surface remained fixed during the calculation in order to simulate atomic bulk positions. The structure was first relaxed using only the gamma point in the first Brillouin zone and afterwards, the calculation was refined by including 8 *k*-points following the Monkhorst–Pack methodology [46]. Finally, the distance between both surfaces is varied until the energy minimum of the most stable interface is found. Additionally, the W(1 1 2) part of the slab has been allowed to relax in the *XY* direction, while keeping the *Z*-coordinate of the last layer fixed, until the most stable structure was found.

In the methodology suggested by von Afthan *et al* to create a grain boundary [47], different numbers of vacancies were created at the interface in order to find the most stable initial configuration. Borovikov *et al* completed this work before for three different W grain boundaries obtaining that, in all the cases, the most stable configurations were free of vacancies [48]. Following this result, we started our analysis with the pure W interface to perform a subsequent energetic study of a metallic vacancy at the grain boundary.

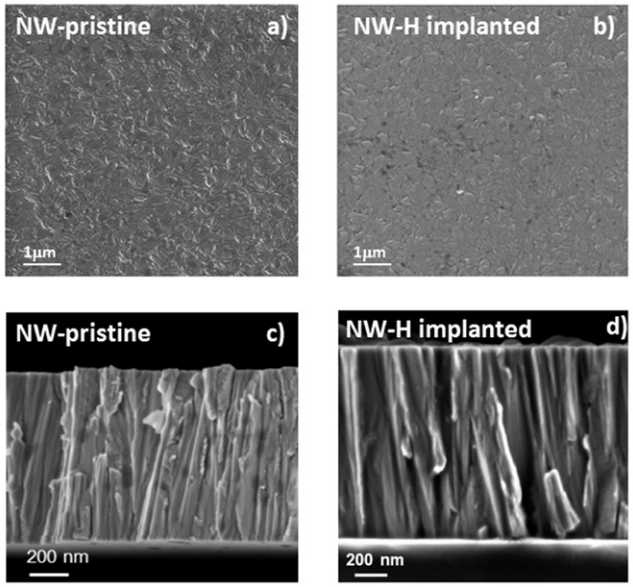

Figure 3. Top view (up) and cross sectional (down) SEM images of a NW coating prior to, pristine, (*a*) and (*c*) and after H implantation (*b*) and (*d*). Nanostructures are preserved after implantation.

The energies obtained for the different structures have been used to estimate the corresponding formation energies. First of all, we should give an appropriate definition for the formation energy in order to have a consistent comparison with the results obtained for systems with periodic conditions in the three directions. The formation energy $E_f(N_H n_{vac})$ of a system wih with n_{vac} W vacancies and N_H hydrogen atoms in the interface is defined as [45]:

$$E_f(N_H n_{vac}) = E_{Tot}(N_H n_{vac}) + n_{vac}E(W) - N_H E(H) - E_{W/W}, \quad (1)$$

where $E_{Tot}(N_H n_{vac})$ is the energy obtained in the relaxation of such interface, $E(W)$ is the energy of one W atom in the bulk, $E(H)$ is half the energy of one isolated H_2 molecule and finally $E_{W/W}$ is the energy of the relaxed clean interface. Equation (1) is equivalent to the one used previously by Yu *et al* [49]. Changing the expression, we can define the solution energy as presented before by Zhou *et al* [31].

$$E_S(N_H n_{vac}) = E_{Tot}(N_H n_{vac}) - N_H E(H) - E_{Tot}(n_{vac}) \quad (2)$$

In a final step, we are interested in the analysis of the defects mobility. For this purpose, we have used the nudged elastic band (NEB) technique [50] as implemented in VASP. This methodology finds the path that minimizes the energetic cost for a displacement between two initial and final geometries. Using this procedure, we can obtain the energy barrier required to jump between two different structures.

3. Experimental results

Figures 3(*a*) and (*c*) show the top view and cross sectional SEM image, respectively, of a pristine NW sample. It is observed that the sample is made of columnar grains which grow perpendicular to the substrate having an average diameter of 100 nm. Moreover, the sample is very compact and does not exhibit any visible cracks. A more detailed description of the morphology and microstructure of NW samples is reported in [36]. As shown in figures 3(*b*) and (*d*), neither the surface morphology nor the columnar structure exhibit any significant change in shape and size after the implantation of hydrogen.

XRD patterns for NW and CGW samples prior to and after H-implantation are depicted in figure 4. All samples exhibit four Bragg peaks corresponding to the α-(1 1 0), α-(2 0 0), α-(2 1 1) and α-(2 2 0) reflections of W. Thus, all studied samples are polycrystalline and mono-phase being made of the stable bcc α-W phase [51]. The main difference in the microstructure between NW and CGW samples is that the first is preferentially oriented along the (1 1 0) direction, whereas the second is preferentially oriented along the (2 0 0) direction. Indeed, by taking a closer look at the XRD patterns of the NW sample, the two main orientations are the (1 1 0) and the (2 1 1). No differences are observed either for the NW-implanted or for the CGW-implanted samples after H implantation.

The projected ranges and the number of target atom displacements, as calculated by the SRIM Monte Carlo code [52], are depicted in figure 5. The displacement energy of W was selected to be 90 eV in the calculations, which is an average value from those reported in the literature [53], and the density of the samples was 19.300 kg m^{-3} [30]. The implantation fluence was 5×10^{20} m^{-2}. As shown in figure 5(*a*) the projected range for the implanted H ions shows a Gaussian-like shape with the peak located at ~680 nm. The maximum number of target atom displacements per incoming ion is around 3.

The measured H depth profiles for NW and CGW coatings implanted with H are depicted in figure 5(*b*). The large H concentration measured at the sample surface (⩽150 nm) mainly relates to surface contamination since the samples were not preserved under vacuum. The fact that the H content at the surface is higher for the CGW than for the NW might be related to the polishing process that these samples underwent prior to implantation. Hence, the H concentration data measured at the sample surface are not considered in the discussion of the results.

The effect of microstructure on H behaviour can be assessed by comparing the H depth profile measured for NW to that for CGW. Very clear differences are observed from the qualitative as well as from the quantitative points of view when comparing the H profiles for the two samples. From the qualitative point of view, the measured depth profile for the NW coating agrees quite well with that calculated, which indicates that hydrogen is mainly retained within the calculated projected range. On the contrary, the depth profile measured for the CGW sample is much broader than that calculated. This might be an indication that in the CGW coating, H diffuses at room temperature (RT). From the quantitative point of view, H retention for the NW sample is significantly larger (1.6×10^{20} at·m^{-2}) than that for the CGW sample (0.9×10^{20} at·m^{-2}). These results illustrate that H retention strongly depends on microstructure. The fact that the H content is higher for the NW than for the CGW sample points out that the NW samples have a larger density of trapping sites than CGW ones. Two reasons can be responsible for such a behaviour. The first

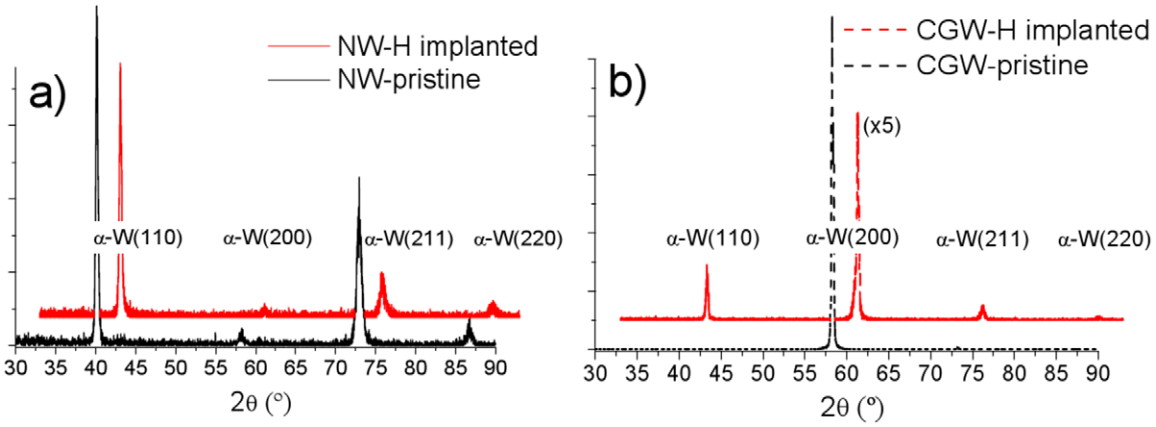

Figure 4. (*a*) XRD patterns for a pristine (black solid line) and implanted with H (red solid line) NW coating and (*b*) the same for a CGW sample.

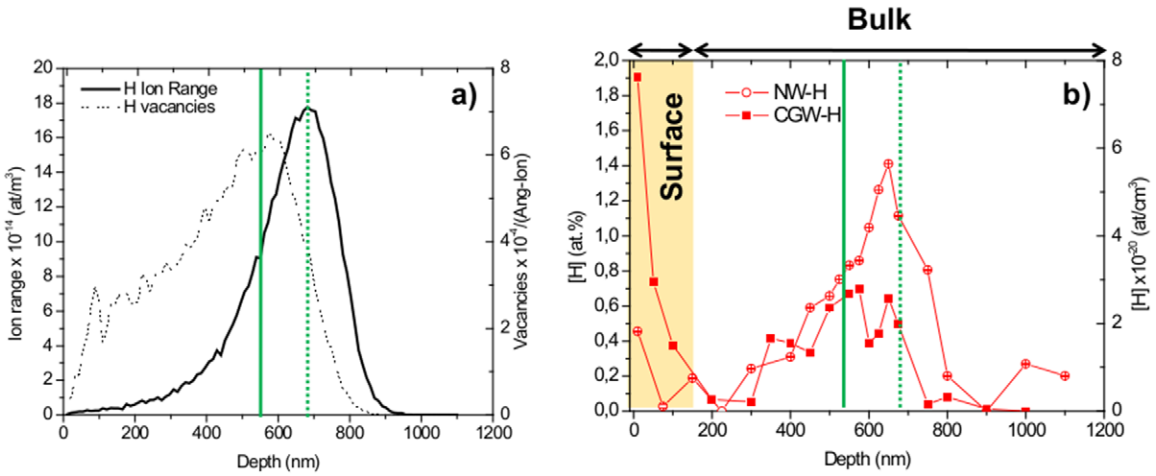

Figure 5. (*a*) H projected range (black solid line) and H-induced vacancy distribution (black dashed line) as calculated by the SRIM Monte Carlo code. (*b*) H depth profiling for NW (red open circles) and for CGW (red filled squares) as estimated from RNRA measurements. The vertical green dashed line in the graph represents the H ion range according to SRIM calculations and the vertical solid green line stands for the centre of the H-induced vacancy peak.

one is to consider that NW samples show enhanced radiation-induced defect generation. Thus, as reported by other authors [54, 55], in nanostructured samples the extremely mobile self interstitial atoms (SIAs) would move to the GB, whereas the immobile vacancies would remain at the interior of the grain. On this basis, the probability for interstitial-vacancy recombination would be smaller in nanostructured than in coarse grained samples. The second reason would be the fact that NW coatings contain trapping sites, apparently homogeneously distributed along the depth as indicated by the retained H profile, which hold H in a very efficient way.

Since the main characteristic of the NW sample is its large density of GBs, one may think that the larger hydrogen retention observed in this sample is related to this fact. Hence, GBs may behave as trapping sites for H. However, because of the diversity of defects (dislocations, vacancies, GBs, ...) in real samples, and considering that all these defects have been reported to trap hydrogen, a straightforward conclusion is not possible and from these data one may only speculate about the role of GBs. On the other hand, computational results reported so far, based on DFT calculations, indicate that GBs behave as pinning sites for hydrogen supporting our speculation [31, 56]. However, as already mentioned these calculations were mainly performed for ideal GBs. Since, as reported by Piaggi *et al* [32], the GB trapping energy depends on the GB type, in order to have a deeper insight about the role of GBs in real samples, DFT calculations were carried out by placing the two preferential directions in the samples that we are dealing with, namely, W(1 1 2) and W(1 1 0), in front of each other. The results are shown in the following section.

4. DFT results

4.1. Structural results

Figure 2 shows the resulting slab after the relaxation of the structure shown in figure 1(*b*) including the 6 layers of metal in both sides. The final reconstruction presents corrugations (difference between the highest and lowest position in the perpendicular direction) of 0.38 Å and 0.06 Å in the first layer of the (1 1 0) and (1 1 2) surfaces, respectively. The first value is

comparable with the corrugations previously obtained in the non-coherent Cu/Nb interface [45] while the latter is appreciably smaller. Interestingly, the corrugation decreases very rapidly in the (1 1 0) surface (0.11 and 0.03 Å in the second and third layer, respectively), and so it can be said that the W atoms converge rapidly to the bulk positions. On the other hand, the corrugation increases in the second layer of the (1 1 2) surface, being 0.18 Å. Highly corrugated interfaces can be expected as good sinks for accumulation of defects, given that the migration barriers could grow. Our low corrugation for the (1 1 2) surface suggests that the opposite behavior could be expected in its vicinity.

Once the interface has been created, one single defect (W vacancy or H atom) was placed at different sites on the interface (see figure 6). The red dotted line define the two dimensional supercell used in the simulations. Then, the system is relaxed under the same conditions previously described. Comparing the energy of each defect at the different positions, the most favorable places for H adsorption and W vacancy formation are found. Notice that the supercell chosen has a $\times 4$ periodicity along the common $\langle 1\,1\,1\rangle$ direction with equivalent sites in each $\times 1$ sub-unit cell. This allows focusing our attention in a small part of the interface.

Initially, the H atoms were implanted over the hollow sites of the W(1 1 0) surface. These points correspond to the tetrahedral positions, where the H atom is preferably accommodated in the bulk as previously reported in many different works [57–60]. In figure 6, the final sites of the H atoms at the interface after relaxation are shown. The three most stable positions are labeled by H_I^1, H_I^2, and H_I^3. In the three cases, the H atom prefers to move closer to the less corrugated (1 1 2) surface. Figure 7(*a*) shows a lateral view of the H_I^1 configuration. The H atom found accommodation between four (almost) equidistant W atoms: two from the (1 1 0) surface, another one from the (1 1 2) surface and the fourth one is located at the second layer of the latter. The distances fall in between 2.01 and 2.04 Å, close to the most stable value obtained for a W–H isolated dimer, namely, 1.7 Å from our calculations. The H atom produced a small deformation (less than 0.04 Å) on the surrounding metallic atoms. This means that the H atom chose a position at the interface where it can interact with several surrounding W atoms so as to minimize the deformation of the system. Additionally, we have checked the stability of a H_2 molecule at the interface. The molecule is dissociated as reported previously for W bulk [60, 61], the W(1 1 0) surface [62] and different symmetric GBs [31, 35].

On the contrary, the change in the atomic positions becomes more important for the most stable V_I^1 vacancy, as shown in figure 7(*b*). It is interesting to notice that this V_I^1 vacancy lies on the same row of the (1 1 2) surface where the H atom was bonded in the previous situation. It means that figures 7(*a*) and (*b*) correspond to exactly the same section of the interface. Now, the atom in the nearest row in the second layer is shifted by 0.52 Å to an intermediate position between the vacancy and its original site. In fact, when the vacancy is created in the second layer, the system evolves to the same structure, showing the great attraction exerted by the interface on the W

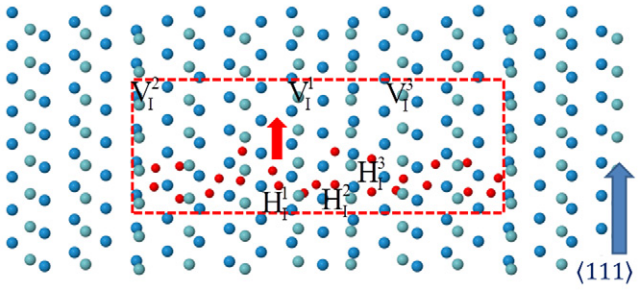

Figure 6. Frontal view of the W(1 1 2)/W(1 1 0) interface shown in figure 1(*b*) after relaxation. Red spheres indicate the different sites where the H atom has been adsorbed, being the three most stable positions denoted as: H_I^1, H_I^2, and H_I^3. In a similar way, the three most stable vacancy positions are denoted as: V_I^1, V_I^2, and V_I^3.

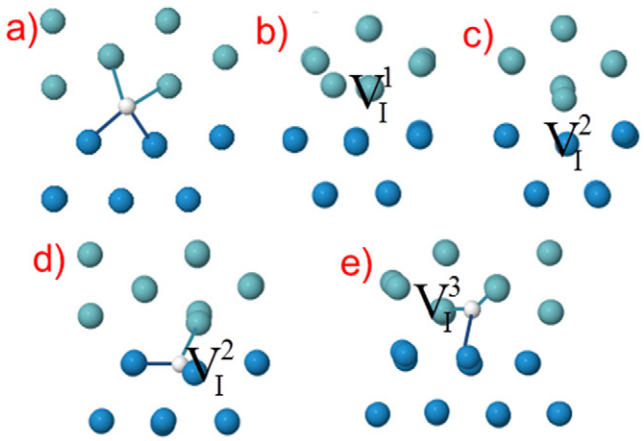

Figure 7. (*a*) Atomic reconstruction around the most stable H position at the interface; (*b*) and (*c*) show the same for a vacancy at the (1 1 2) and (1 1 0) surface, respectively; (*d*) and (*e*) show the most stable H positions when vacancies V_I^2 and V_I^3 are present, respectively.

vacancies at the (1 1 2) side. On the other hand, the most stable vacancy on the (1 1 0) side is placed on the row denoted as V_I^2 in figure 6. The atomic configuration around such a vacancy is depicted in figure 7(*c*). Again, a first neighbor atom moves 0.52 Å to an intermediate position, but in this case the atom comes from the opposite surface. Interestingly, when the vacancy is created in the corresponding row of the (1 1 2) surface, something similar happens to the nearby atom in the (1 1 0) surface: it moves 0.52 upwards, closer to the (1 1 2) layer. In both cases, the final structure has similar energy.

Finally, the most stable V_I^1, V_I^2 and V_I^3 vacancies have been filled in with a H atom. The hydrogen does not occupy the vacancy site, in agreement with the result found by Zhou *et al* in their symmetric GB [31] and following the same tendency than in the bulk [59, 60]. In the three cases analyzed, the H occupies a different position at the interface than in the equivalent case without the vacancy, moving closer to the nearest surface. Contrary to what can be expected, the most stable cases are obtained when the H atom is placed near the V_I^2 and the V_I^3 sites, see figures 7(*d*) and (*e*). In both cases, the H atoms are bonded with three surrounding W atoms. In the first case, figure 7(*d*),

Table 1. Formation energies (in eV) of one H, one vacancy (V) and one H in a vacancy (HV) for the three most stable cases obtained at the interface (Int) as compared to bulk results (bulk) and other works (Int-bib and bulk-bib).

	Int[1, 2, 3]	Int-bib	Bulk	Bulk-bib
$E_f(H)$	− 0.09,−0.07,−0.05	− 1.73,−0.13 [49]	0.96	0.85 [49]
$E_f(V)$	1.51, 1.57, 1.64	3.66, 2.36 [35]	3.16	3.11 [63], 3.52 [58]
$E_f(HV)$	1.44, 1.21, 1.20	—	2.80	2.86 [59, 60]*
$E_S(H)$	− 0.09,−0.07,−0.05	− 0.23 [31]	0.96	0.89 [31]
$E_S(V)$	− 0.05,−0.35,−0.42	− 0.63 [31]	− 0.25	− 0.31 [31]

Note: The 1, 2, 3 indices identify the corresponding three cases analyzed here for H, V and HV. *The value was estimated combining the energies presented in both works.

the H is bonded with two W atoms from the first layer of the (1 1 0) surface (each one placed in different rows) and a third atom located in the first layer of the (1 1 2) surface. The three W atoms lie at equidistant distances from the H (1.92 Å). In the second geometry, figure 7(*e*), the closest W atom (1.97 Å) sits at the second layer of the (1 1 2) surface, underneath there is a W atom at the (1 1 0) surface at 2.06 Å and finally the third W atom lies in the same row as the vacancy V_I^3 at 2.38 Å.

4.2. Energetic analysis

Once the most stable structures have been found, an energetic analysis needs to be performed to compare the formation energy of the most stable structures to previous bulk simulations or calculations for other GBs. The equations (1) and (2) are used to estimate the corresponding formation and solution energies for the different cases analyzed in the previous section. The resulting values are summarized in table 1.

The three formation energies obtained for the H_I^1, H_I^2 and H_I^3 sites are clearly smaller than the value obtained in a bulk calculation (performed for a $5 \times 5 \times 5$ cubic unit cell using the same parameters than in [64]). The results suggest that H finds a more comfortable place to stay at the interface (−0.09 eV versus 0.96 eV). The same conclusion was previously found by several authors [31, 32, 49, 59]. We can directly compare the solution energies obtained by Zhou *et al* using the symmetric 36.9° [1 0 0]{0 1 3}$\Sigma = 5$ [31]. Notice that for a H atom placed at the interface the formation energy defined in equation (1) is the same than the solution energy of the equation (2). The values for the three most stable cases are lower than in that work (−0.09 eV versus −0.23 eV), suggesting that the symmetric GB attracts H more strongly than this non-coherent interface. We have performed an additional simulation implanting the H atom in the second layer of each surface near the most stable positions. In the (1 1 2) case, the atom moves directly to the interface, finally occupying the H_I^1 site. On the contrary, the H in the second layer of the (1 1 0) surface stays in a meta-stable tetrahedral position with an energy higher than that at the first layer by about 0.87 eV, but still a little bit more stable than the bulk value. This means that the H atoms will tend to move to the GB whenever possible. In principle, if no motion of H along the GB is considered, this result may account for the experimental results that indicate that hydrogen concentration after implantation is larger for the NW than for the CGW.

From an inspection of table 1, we can conclude that, as happened before with the H atoms, vacancies are attracted to the interface. The formation energy of the three most stable vacancies is clearly lower than the value obtained in the bulk (1.51 versus 3.16 eV) as well as lower than the result obtained for a $\Sigma = 3\langle 1\,1\,1\rangle$ tilt grain boundary [35]. Consequently, the vacancies are expected to be located at the GBs too. Again, we can create the defect in the second layer of each surface. As mentioned before, the vacancy in the (1 1 2) second layer evolves to the same position as when it is initially in the first layer, revealing its great tendency to find the interface, whereas on the (1 1 0) surface the vacancy is stable at the second layer, being the resulting energy 1.10 eV higher than in the first layer. As for the H case, the resulting formation energy (2.66 eV) lies in between the interface and the bulk cases. So, again it can be expected that the vacancy will try to move to an interfacial position.

Additionally, we have studied the relative stability of the complex (HV) formed by a H atom and a metallic vacancy in different configurations. In table 1, the formation energies of H in the three vacancies are presented resulting the V_I^3 vacancy as the most stable site followed by the V_I^2 by around 10 meV. Once again, the three values are much lower than in the bulk, confirming the great attraction of both defects even when they are together at the interface. The solution energy obtained by Zhou *et al* [31] is again lower than the values presented here (−0.63 eV versus −0.42 eV), thus confirming a greater attraction from the symmetric GB than from the analyzed interface. We have performed different simulations including one H and a metallic vacancy separated at the interface. For example, we have tried the structure with a vacancy in the most stable V_I^1 site and an additional H atom in two possible positions: in the same row but far away from the vacancy and in the H_I^2 site. Both final structures are 0.22 and 0.36 eV less stable, respectively, than the geometry presented in figure 7(*d*). Thus, although the H atoms do not occupy exactly the vacancy site, the system finds a better accommodation when both defects are close to each other. This tendency could imply that the H atoms will accumulate near the vacancies at the GB reducing the damage in the interface and consequently extending the service life of the material.

4.3. Mobility of defects

In a final step, we have studied the mobility of the defects at the interface. Due to the special configuration created, the defects are expected to move in the interface along the rows in the ⟨1 1 1⟩ direction as suggested in figure 6. For that purpose, we have performed calculations based on the NEB technique [50] mentioned in section 2.2 to obtain the energy barrier required to jump between two different structures. For one H atom, we started from the most stable H_I^1 site. In the same row, a second almost equivalent structure was found to be only 10 meV less stable. The resulting migration energy between these two points is just 0.12 eV, a value smaller than the one obtained in a similar simulation between two tetrahedral sites in the perfect bulk (0.21 eV). This result suggests that the H atoms will move more easily along this interface than in the perfect bulk, in good agreement with previous findings for different symmetrical GBs [31, 32, 35]. Additionally, we have studied how the H atom reaches the interface, performing a NEB calculation between the most stable site at the interface and the geometry with the H in the second layer. As mentioned before, in the W(1 1 2) surface the H atom moves directly from the second layer to the interface, so we have only performed the NEB for the W(1 1 0) surface. The resulting migration energy is 0.15 eV, again lower than in the bulk, showing the great attraction exerted by the interface on the H atoms. This result suggests that the H atoms will move faster as they approach the interface, justifying the H accumulation at the GB suggested by the experimental results.

Regarding vacancies, in both sides of the interface they are expected to jump between first neighboring positions. For simplicity, we have analyzed the motion along the rows shown in figure 6, where all the positions are equivalent and the atoms jumps between first neighboring positions. For other alternative motions, the vacancy will jump from one row to another chain where the formation energy is higher; therefore, the barrier is expected to be higher. Then, the migration energy is calculated along the V_I^1 and V_I^3 rows for the (1 1 2) and (1 1 0) surfaces, respectively. The barriers were estimated to be 1.16 and 0.75 eV, lower than the 1.70 eV presented in [65]. Although the value is much higher than for H migration, we can conclude again that the vacancy can move along the interface more easily than in the bulk. As mentioned before, a vacancy in the second layer at the (1 1 0) surface is more than 1 eV less stable than in the first layer. Interestingly, the calculated energy barrier is really small, around 20 meV. Consequently, recalling that the vacancy in the second layer of the (1 1 2) surface evolves to a similar structure to the case in the first layer, it will migrate very easily to the first layer in both surfaces, thus confirming again the great tendency of vacancies to move to the interface.

Finally, we estimated the energetic cost for a H atom to escape (or dissociate) from a monovacancy in the interface. A lower bound can be obtained comparing the energies of the structures with the H atom inside/outside the vacancy. As mentioned in the previous section, the energy difference between these configurations is 0.22 eV. To this values we should add the energy barrier that the H atom has to jump during the migration process. This calculation implies a very complex NEB simulation, but a reasonable value could be close to the migration energy of the H at the interface. Then, the final energy cost will be around 0.35 eV, resulting in a barrier higher than in the bulk. This result suggests one of the mechanisms that explain the larger H retention in the GB, but at the same time hints that hydrogen could be easily removed from the material.

5. Conclusions

In summary, experimental results show that nanostructured tungsten samples with a columnar structure and a large number of (1 1 0)/(1 1 2) interfaces retain more hydrogen than coarse grained tungsten samples. One plausible explanation for such a behavior is to consider that hydrogen is trapped at grain boundaries. Based on the density functional theory, our calculations carried out for a realistic non-coherent W(1 1 0)/W(1 1 2) interface confirm this speculation. The results show that H atoms find a better accommodation near the vacancy at the interface than anywhere in the bulk or even than at the pure interface. This should be one of the mechanisms explaining the high H accumulation experimentally measured for nanostructured tungsten samples. The formation of the HV complexes is favored by the strong attraction exerted by these interfaces to H atoms and single vacancies and the low migration energies found for both kind of defects along the interface. Indeed, the relatively low energy estimated for the H-V dissociation may favor the subsequent H outdifussion. Hence, the theoretical results support the experimental findings, making the nanostructured tungsten an attractive alternative for the potential plasma facing material. Moreover, this work contributes to account for the role of each kind of defect in the hydrogen behavior, which is required to validate simulations and to use them for further realistic predictions of material behavior under conditions which experimentally cannot be reached so far like those taking place in a nuclear fusion reactor.

Acknowledgments

This work has been supported by the FP7 project RADINTERFACES and the Spanish Ministry of Economy and Competitiveness projects NANO-EXTREM MAT2012-38541-C02-01 and 02 and RADIAFUSS ENE-2012-39787-CO6. The authors acknowledge the computer resources by the Spanish Supercomputing Network (RES), project FI-2014-3-0005 and the European PRACE-3IP project (FP7 RI-312763) resources Fionn based in Ireland at ICHEC and Supernova based in Poland at the Wroclaw University of Technology. Research by NG is supported by MINECO (Spain) under project JdC-2012.

References

[1] ITER Physics Basis Editors *et al* 1999 *Nucl. Fusion* **39** 2137
[2] Anklam T.M., Dunne M., Meier W.R., Powers S. and Simon S. 2011 *Fusion Sci. Technol.* **60** 66–71
[3] Perlado M. *et al* 2011 *Proc. SPIE* **8080** 80801Z
[4] Kaufmann M. and Neu R. 2007 *Fusion Eng. Des.* **82** 521

[5] Raffray A.R., Haynes D. and Najmabadi F. 2003 *J. Nucl. Mater.* **313–316** 23–31
[6] Barabash V. *et al* 1996 *J. Nucl. Mater.* **233** 718
[7] Alvarez J. *et al* 2011 *Fusion Sci. Technol.* **60** 565 (http://www.ans.org/pubs/journals/fst/a_12443)
[8] Ueda Y. 2010 *Plasma Fusion Res.* **5** S1009
[9] Causey R.A. and Venhaus T.J. 2001 *Phys. Scr.* **T94** 9–15
[10] Zayachud Y., Manhard A., 't Hoen M.H.J., Jacob W., Zeijlmans van Emmichoven P.A. and van Oos G. 2014 *Nucl. Fusion* **54** 123013
[11] Tokunaga K. *et al* 2005 *J. Nucl. Mater.* **337–9** 887
[12] Ueda Y. *et al* 2005 *J. Nucl. Mater.* **337–9** 1010
[13] Rieth M. *et al* 2013 *J. Nucl. Mater.* **432** 482
[14] Khedir K.R., Kannarpady G.K., Ishihara H., Woo J., Ryerson C. and Biris A.S. 2010 *Phys. Lett.* A **374** 4430
[15] Kim Y., Hong M.-H., Ho Lee S., Kim E.-P., Lee S. and Noh J.-W. 2006 *Met. Mater. Int.* **12** 245
[16] Yar M.A., Wahlberg S., Bergqvist H., Salem H.G., Johnsson M. and Muhammed M. 2011 *J. Nucl. Mater.* **408** 129
[17] Kurishita H., Matsuo S., Arakawa H., Sakamoto T., Kobayashi S., Nakai K., Takida T., Kato M., Kawai M. and Yoshida N. 2010 *J. Nucl. Mater.* **398** 87
[18] Veleva L. 2011 Contribution to the production, characterization of W-Y, W-Y2O3 and W-TiC materials for fusion reactors *Thesis* EPFL no. 4995
[19] Wurster S. *et al* 2013 *J. Nucl. Mater.* **442** S181–9
[20] López-Ruiz P., Ordás N., Iturriza I., Walter M., Gaganidze E., Lindig S., Koch F. and García-Rosales C. 2013 *J. Nucl. Mater.* **442** S219–24
[21] Shu W.Mo., Luo G.-N. and Yamanishi T. 2007 *J. Nucl. Mater.* **367–70** 1463–7
[22] Hasegawa T., Tomita Y. and Kohyama A. 1998 *J. Nucl. Mater.* **258–63** 1153
[23] Klueh R.L., Ehrlich K. and Abe F. 1992 *J. Nucl. Mater.* **191–4** 116
[24] Klueh R.L. *et al* 2002 *J. Nucl. Mater.* **307–11** 455
[25] Bai X.-M., Voter A.F., Hoagland R.G., Nastasi M. and Uberuaga B.P. 2010 *Science* **327** 1631
[26] Ackland G. 2010 *Science* **327** 1587
[27] Aucouturier M. 1982 *J. Phys. Colloq.* **43** C6-175–86
[28] Ueda Y., Kashiwagi H., Fukumoto M., Ohtsuka Y. and Yoshida N. 2009 *Fusion Sci. Technol.* **56** 85 (http://www.ans.org/pubs/journals/fst/a_8881)
[29] González-Arrabal R. *et al* 2014 *J. Nucl. Mater.* **453** 287
[30] Ogorodnikova O.V., Tyburska B., Alimov V.K. and Ertl K. 2011 *J. Nucl. Mater.* **415** S661–6
[31] Zhou H.-B. *et al* 2010 *Nucl. Fusion* **50** 025016
[32] Piaggi P.M. *et al* 2015 *J. Nucl. Mater.* **458** 233
[33] Zhou H.-B. *et al* 2010 *Nucl. Fusion* **50** 115010
[34] Lu G-H., Zhou H-B. and Becquart C.S. 2014 *Nucl. Fusion* **54** 086001
[35] Xiao W. and Geng W.T. 2012 *J. Nucl. Mater.* **430** 132–6
[36] Gordillo N. *et al* 2014 *Appl. Surf. Sci.* **316** 1–8
[37] Alvarez J., Garoz D., González-Arrabal R., Rivera A. and Perlado J.M. 2011 *Nucl. Fusion* **51** 053019
[38] Tesmer J.R. and Nastasi M.A. 1995 *Handbook of Modern Ion Beam Materials Analysis* (Pittsburgh, PA: Materials Research Society)
[39] Chernov I.P., Mamontov A.P., Tjurin Y.I. and Cherdantsev Y.P. 1996 *J. Nucl. Mater.* **233–237** 1118–22
[40] González-Arrabal R. *et al* 2012 *Nucl. Instrum. Meth.* B **271** 27
[41] Kresse G. and Hafner J. 1993 *Phys. Rev.* B **47** R558
Kresse G. and Furthmuller J.J. 1996 *Phys. Rev.* B **54** 11169
Kresse G. and Joubert D. 1999 *Phys. Rev.* B **59** 1758
[42] Perdew J.P., Burke K. and Ernzerhof M. 1996 *Phys. Rev. Lett.* **77** 3865
[43] Blöchl P.E. 1994 *Phys. Rev.* B **50** 17953
[44] James A.M. and Lord M.P. 1992 *Macmillan's Chemical and Physical Data* (Basingstoke: Macmillan)
[45] González C., Iglesias R. and Demkowicz M.J. 2015 *Phys. Rev.* B **91** 064103
[46] Monkhorst H.J. and Pack J.D. 1976 *Phys. Rev.* B **13** 5188
[47] von Alftan S., Haynes P.D., Kaski K. and Sutton A.P. 2006 *Phys. Rev. Lett.* **96** 055505
[48] Borovikov V., Tang X.-Z., Perez D., Bai X.-M., Uberuaga B.P. and Voter A.F. 2013 *Nucl. Fusion* **53** 063001
[49] Yu Y., Shu X., Liu Y.N. and Lu G.H. 2015 *J. Nucl. Mater.* **455** 91–5
[50] Jonsson H., Mills G. and Jacobsen K.W. 1998 *Classical and Quantum Dynamics in Condensed Phase Simulations* ed B.J. Berne *et al* (Singapore: World Scientific) p 385
[51] Vink T.J. *et al* 1993 *J. Appl. Phys.* **74** 988
[52] Ziegler J.F., Ziegler M.D. and Biersack J.P. 2010 *Nucl. Instrum. Methods Phys. Res.* B **268** 1818
[53] 't Hoen M.H.J. *et al* 2012 *Nucl. Fusion.* **52** 023008
[54] Samaras M., Derlet P.M., Van Swygenhoven H. and Victoria M. 2006 *J. Nucl. Mater.* **351** 47
[55] Fu C.-C. and Willaime F. 2004 *Phys. Rev. Lett.* **92** 175503
[56] von Toussaint U. *et al* 2011 *Phys. Scr.* **T145** 014036
[57] Juslin N. *et al* 2005 *J. Appl. Phys.* **98** 123520
[58] Li X.C., Shu X., Liu Y.N., Gao F. and Lu G.H. 2011 *J. Nucl. Mater.* **408** 12
[59] Liu Y.-L., Zhang Y., Luo G.-N. and Lu G.-H. 2009 *J. Nucl. Mater.* **390–391** 1032–4
[60] Liu Y.L., Zhang Y., Zhou H.B., Lu G.H., Liu F. and Luo G.N. 2009 *Phys. Rev.* B **79** 172103
[61] Becquart C.S. and Domain C. 2009 *J. Nucl. Mater.* **385** 223
[62] Nojima A. and Yamashita K. 2007 *Surf. Sci.* **601** 3003–11
[63] Becquart C.S. and Domain C. 2007 *Nucl. Instrum. Methods Phys. Res.* B **255** 23
[64] González C., Cerdeira M.A., Palacios S.L. and Iglesias R. 2015 *J. Mat. Sci.* **50** 3727–39
[65] González C. and Iglesias R. 2014 *J. Mater. Sci.* **49** 8127